processes

MDPI

Article

The Hydrodynamics of a Rod-Shaped Squirmer near a Wall

Hao Ye [1], Jianzhong Lin [2,*] and Zhenyu Ouyang [1]

[1] State Key Laboratory of Fluid Power Transmission and Control, Zhejiang University, Hangzhou 310027, China
[2] Zhejiang Provincial Engineering Research Center for the Safety of Pressure Vessel and Pipeline, Ningbo University, Ningbo 315201, China
* Correspondence: mecjzlin@public.zju.edu.cn; Tel.: +86-571-87952882

Abstract: The hydrodynamic characteristics of a rod-shaped squirmer swimming near a wall were studied numerically using the immersed boundary-lattice Boltzmann method in the swimming Reynolds number range of $0.1 \leq Re_s \leq 2.0$, where the number of assembled squirmers was $2 \leq i \leq 4$ and the distance between two adjacent assembled squirmers was $0.75\ d \leq s \leq 1.5\ d$ (d is the diameter of a single squirmer). The effect of Re_s, i and s on the swimming mode of the squirmer was explored. The results showed that there are four swimming modes after the first collision between the rod-shaped squirmer and the wall. There are also four swimming modes when Re_s changes from 0.1 to 2.0. Puller, pusher and neutral squirmers showed different swimming modes when i changed, and the effect degree of the flow at the previous moment on the squirmer's motion was different for different values of i. The change in s only affected the trajectory of the squirmer without changing its motion mode. Puller, pusher and neutral squirmers showed different swimming modes and velocity changes when s changed.

Keywords: squirmer; rod-shaped; swimming mode; trajectory; azimuth angle; simulation

Citation: Ye, H.; Lin, J.; Ouyang, Z. The Hydrodynamics of a Rod-Shaped Squirmer near a Wall. *Processes* **2022**, *10*, 1841. https://doi.org/10.3390/pr10091841

Academic Editors: Lutz Böhm, Matthias Kraume and Michael Schlüter

Received: 27 August 2022
Accepted: 10 September 2022
Published: 13 September 2022

1. Introduction

Situations of microorganisms swimming are everywhere in nature and industrial applications. In contrast to large organisms such as birds, fishes or insects, which achieve their locomotion by imparting momentum to the fluid, microorganisms swim using one or more appendages including flagella (*E. coli* and spermatozoa), cilia (Paramecium) or cell deformation (*Borrelia burgdorferi*) by viscous force in a flow with a low Reynolds number [1]. For example, spermatozoa travel in the female reproductive tract through flexible filament whipping [2]. *Escherichia coli* moves to the nutritive region in the guts through stiff helix rotation [3], and alga can swim forward or in reverse with two flagella by using ciliary and flagellar beat strategies, respectively [4]. Microorganisms frequently collide with passive particles as well as solid boundaries in flows, which is relevant in numerous biological phenomena. Therefore, the investigation of the motion of microorganisms near a wall is of great importance and may be beneficial in biomedical and engineering applications.

Previous experiments have observed various swimming behaviors for microorganisms near a boundary, such as the stable "dancing" states of Volvox [5], the backward swimming of spermatozoa [6], the circular trajectories of Escherichia coli [7] and the biofilm formation of bacteria attached to a surface [8]. Some simplified models have been proposed for studying the hydrodynamics of swimmers in the vicinity of a wall. Or and Murray [9] have studied the dynamic stability of swimmers comprised of rotating spheres and rigid rods near a plane wall. They found the existence of stable periodic motion and passively stable conditions along the wall when the structure of the swimmer changed. Zargar et al. [10] investigated the influence of a wall on the dynamics of a three-sphere swimmer moving through varying the length of its arms in a periodic manner. Their results showed that for different initial angles and distances from the wall, there were four swimming modes. In particular, the swimmer oriented its head toward the wall when the initial angle was slightly

negative in the near-wall phase. Dunstan et al. [11] presented a two-sphere model for bacteria swimming near a solid surface. The results showed that three different swimming modes depended on the initial conditions: swimming in circles in contact with the wall, swimming in circles at a finite distance from the wall and swimming away from the wall. Pimponi et al. [12] also found the counterclockwise trajectory of a flagellated microorganism by using the boundary element method, which was in agreement with the experimental results of Leonardo et al. [13].

Recently, the "squirmer" model has been widely used to investigate the hydrodynamics of self-propelled swimmers. Paravassiliou and Alexander [14] illustrated the reciprocal theorem for a squirmer near a solid surface and extended it to a general squirming set. Lintuvuori et al. [15] studied the hydrodynamics of a fully resolved squirmer confined between two walls, and the results showed that a pusher moved faster when it was close to a surface than in the bulk, whereas a puller underwent a transition between fast motion and a dynamical standstill. Li and Ardekani [16] simulated a squirmer near a wall by a distributed Lagrange-multiplier-based finite-volume method and found three different swimming modes, i.e., escaping from the wall, swimming along the wall at a constant distance and orientation angle, and swimming near the wall in a periodic trajectory. Ishimoto and Gaffney [17] theoretically explored the boundary behavior of axisymmetric squirmers for a no-slip interface and also a free surface with the small capillary number limit, preventing leading-order surface deformation, and suggested the necessity of surface deformation for stable three-dimensional free-surface finite-size microswimming. Poddar et al. [18] illustrated how the near-wall swimming velocities are non-trivially altered by the interaction of wall slip and hydrodynamic forces, and reported a characteristic transition of swimming trajectories for both puller- and pusher-type microswimmers by hydrodynamic slippage if the wall slip length crossed a critical value. Ouyang et al. [19] numerically studied the hydrodynamic properties of a squirmer swimming in a power-law fluid near a wall using an immersed boundary-lattice Boltzmann method considering the effect of the power-law index, the Reynolds number, the initial orientation angle and the initial distance of a squirmer from the wall, and found four new swimming modes. In the shear-thinning fluid, both pushers and pullers with a larger β would display the phenomenon of reverse swimming near the wall. Kuron et al. [20] theoretically and numerically studied the hydrodynamic behaviors of a squirmer bounded by spherical objects and walls using the reflection method, and found that backward sliding behavior for sufficiently strong pushers was caused by the strong forces opposing forward motion generated from the fluid recirculation between the squirmer and the wall. Pietrzyk et al. [21] calculated the non-Newtonian correction of the flow analytically with the asymptotic limit of a small Carreau number, and the results showed cases where the non-local effect could be more significant than the local effect. They also suggested that caution should be exercised when developing physical intuition from the local viscosity distribution alone around a swimmer in a shear-thinning fluid. Eastham and Shoele [22] studied the ciliary locomotion and feeding of an axisymmetric microswimmer in a complex fluid whose viscosity depended on the surrounding nutrient field, and the results demonstrated that non-local effects from variation in the viscosity were caused by a modification of the pressure force, as opposed to the strain rate. Van Gogh et al. [23] examined the effects of geometrical shape upon locomotion in a shear-thinning fluid, and the results showed the advantages of spheroidal over spherical swimmers in terms of both swimming speed and energetic efficiency when squirming through a shear-thinning fluid, and the possibility of tuning the swimmer's geometry to better exploit non-Newtonian theological behaviors for more effective locomotion in complex fluids.

Actually, in the world of microorganisms, there are a variety of species with wide diversity in their body shapes, e.g., Bacillus is rod-like, and Spiroplasma presents an elongated shape with flexibility. Ouyang and Lin [24] proposed a model of rod-shaped squirmers to investigate the hydrodynamics of elongated swimmers. A rod-shaped squirmer consists of several spherical squirmers in tandem. Ouyang et al. [25] studied the hydrodynamics of an inertial squirmer and a squirmer dumbbell in a tube, and found that the fluid's

inertia affected the swimming stability of the squirmers and the squirmer dumbbells; the pusher would swim in the opposite direction, accompanied by periodic oscillation, and its amplitude increased with an increase in the Reynolds number. Li and Ardekani [16] presented numerical results for the steady speed of a squirmer swimming in an unbounded fluid, and showed that the swimming speed of pullers and pushers changed with the Reynolds number.

By reviewing previous relevant research, it can be seen that research on the effects of the distance between two adjacent squirmers, the number of assembled squirmers and the Reynolds number on the hydrodynamics and swimming mode of rod-shaped squirmers is lacking. Therefore, in the present work, we studied the hydrodynamics of a rod-shaped squirmer swimming near a wall at a finite Reynolds number by using the immersed boundary-lattice Boltzmann method [26], and explored the hydrodynamic characteristics and swimming mode of squirmers when some parameters of the flow and the squirmer changed.

2. Numerical Method and Validation

2.1. Rod-Shaped Squirmer Model

The spherical squirmer, as an archetypal model of swimmers based on the Stokes theory, was presented by Lighthill [27], modified by Blake [28] and further developed by other studies, and has been widely used to simulate the locomotion of ciliated organisms such as Volvox, Oplina and Paramecium. The simplified form of a two-dimensional squirmer, i.e., only the tangential velocity on the surfaces drives the body, was adopted to assemble the rod-shaped squirmer:

$$\boldsymbol{u}_\theta|_{r=a} = (B_1 \sin\theta + 2B_2 \sin\theta\cos\theta)\boldsymbol{e}_\theta \quad (1)$$

where θ is the angle in polar coordinates measured from the self-propulsion direction, $\boldsymbol{e}_\theta$ is the unit vector along the θ direction of the squirmer, and B_1 and B_2 are constants. On the right-hand side of Equation (1), the first term determines the swimming velocity $U|_{Re=0} = B_1/2$ and the second term presents the intensity of the vorticity around the surface of the squirmer. Three kinds of squirmer were specified in the light of the values of $\beta = B_2/B_1$ with $B_1 > 0$, i.e., $\beta > 0$ denotes a puller (Chlamydomonas), inducing thrust in front of the swimmer; $\beta < 0$ denotes a pusher (spermatozoa), inducing thrust at the rear of the swimmer; and $\beta = 0$ denotes a neutral squirmer (Paramecium). A rod-shaped squirmer was assembled jointly by several squirmers with identical posture, i.e., with the same orientation as shown in Figure 1a, where the red arrows represent the orientation of each squirmer. Similar to a single squirmer, a rod-shaped squirmer can be categorized as a puller ($\beta > 0$), pusher ($\beta < 0$) or neutral ($\beta = 0$) squirmer. Each rod-shaped squirmer motivates itself with the same distribution of the surface velocity. Rod-shaped squirmers with different shapes or configurations were created by altering the distance between two neighboring squirmers and the number of assembled squirmers, which could model diverse species of microorganisms. Furthermore, this model of rod-shaped squirmer can be modified to a rod-like model of flexibility to mimic the swimmers with deformable and elongated shapes [24].

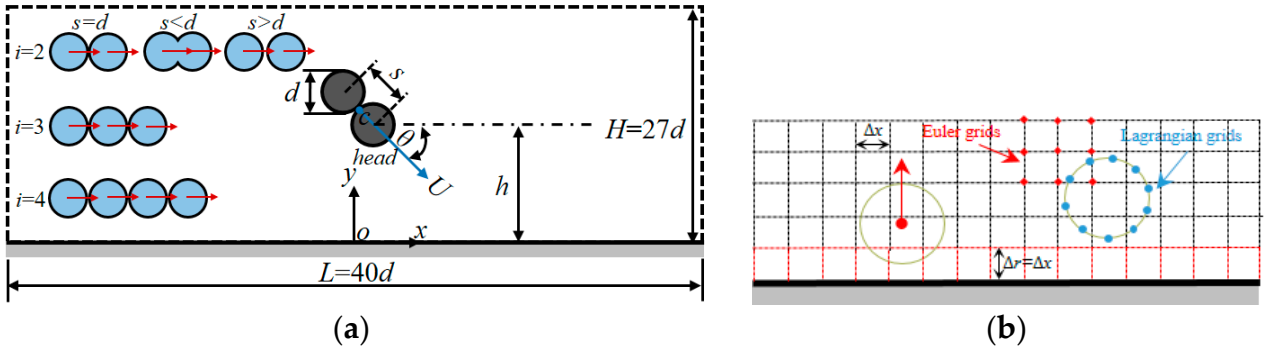

Figure 1. Schematic diagram of the flow. (**a**) Rod-shaped squirmer near the wall; (**b**) lattice.

The rod-shaped squirmer is assumed to be rigid, and its motion is governed by Newton's second law:

$$M\frac{d^2\boldsymbol{x}_c}{dt^2} = \boldsymbol{F}, \tag{2}$$

$$\frac{d(J\cdot\boldsymbol{\Omega})}{dt} = \boldsymbol{T}, \tag{3}$$

where M and $\boldsymbol{x}_c$ are the mass and centroid position of the squirmer, J and Ω are the moment of inertia and the angular velocity of the squirmer, and $\boldsymbol{F}$ and $\boldsymbol{T}$ represent the force and torque exerted on the squirmer, respectively. In the static coordinates, the distribution of the velocity at the surface of the squirmer is given by

$$\boldsymbol{u}_s = \boldsymbol{U} + \boldsymbol{\Omega}\times\boldsymbol{x}_s + \boldsymbol{u}_\theta, \tag{4}$$

where $\boldsymbol{U}$ is the translational velocity and $\boldsymbol{x}_s$ indicates the vector pointing from the centroid of a squirmer to its surface.

When two squirmers swam in the flow, we kept the distance between the centroid of two squirmers unchanged according to the law of rigid-body motion, so two squirmers remained connected to a form a rod-shaped squirmer.

2.2. Repulsive Force Model

When the squirmer swam towards the near-wall region and then collided with the solid boundary, the model of short-range repulsive force was used to prevent non-physical overlaps between the squirmer and the wall. The model was presented by Glowinski et al. [29] and given as:

$$\boldsymbol{F}_r = \frac{C_m}{\varepsilon}\left(\frac{d-d_{\min}-\Delta r}{\Delta r}\right)^2\boldsymbol{e}_r, \tag{5}$$

where $C_m = MU_p/a$ is the characteristic force; M and U_p are the mass and velocity of the centroid of the squirmer, respectively; a is the radius of a single squirmer; $\varepsilon = 10^{-4}$ is a small invariable; d is the distance between the squirmer and the wall; d_{min} denotes the minimum possible distance; $\Delta r = \Delta x$ indicates that the repulsive force only exits in the one-lattice sized region near the wall, as shown in Figure 1b, where Δx is the size of the lattice; and $\boldsymbol{e}_r$ denotes the direction of the repulsive force which is perpendicular to the wall.

2.3. Immersed Boundary-Lattice Boltzmann Method

The numerical simulations were conducted using the direct forcing immersed boundary-lattice Boltzmann (IB-LB) method [30]. The continuity and momentum equations for the flow are:

$$\nabla\cdot\boldsymbol{u} = 0, \tag{6}$$

$$\frac{\partial\boldsymbol{u}}{\partial t} + (\boldsymbol{u}\cdot\nabla)\boldsymbol{u} = -\frac{\nabla p}{\rho} + \frac{\mu}{\rho}\nabla^2\boldsymbol{u} + f, \tag{7}$$

where $\boldsymbol{u}$, p, ρ, μ and $\boldsymbol{f}$ are the fluid velocity, pressure, density, viscosity and external body force on the fluid, respectively.

When an external force exits, the discrete lattice Boltzmann equation (LBE) can be derived and given in the following explicit form [31]:

$$f_\alpha(\boldsymbol{x}+\boldsymbol{e}_\alpha\Delta t, t+\Delta t) = f_\alpha(\boldsymbol{x},t) - \frac{1}{\tau}[f_\alpha(\boldsymbol{x},t) - f_\alpha^{eq}(\boldsymbol{x},t)] + F_\alpha(\boldsymbol{x},t), \tag{8}$$

where Δt is the lattice time, τ is the relaxation time, $f_\alpha(\boldsymbol{x}, t)$ is the distribution function at position $\boldsymbol{x}$ and time t for the discrete velocity in the direction $\boldsymbol{e}_\alpha$ and $f_\alpha{}^{eq}(\boldsymbol{x}, t)$ is the equilibrium distribution function given by

$$f_\alpha^{eq}(\boldsymbol{x},t) = \rho\omega_\alpha[1 + \frac{3}{c^2}(\boldsymbol{e}_\alpha\cdot\boldsymbol{u}) + \frac{9}{2c^4}(\boldsymbol{e}_\alpha\cdot\boldsymbol{u})^2 - \frac{3}{2c^2}\boldsymbol{u}^2], \tag{9}$$

where c is the lattice speed and $c^2 = 3{c_s}^2$ with c_s being the speed of sound. In our simulation, the lattice size $\Delta x = 1$ and the lattice time $\Delta t = 1$, so the lattice speed was derived as $c = \Delta x/\Delta t = 1$. Here, $c^2 = 3{c_s}^2$ was the result of derivation of the two-dimensional nine-speed model (D2Q9).

The D2Q9 model was used here for simulations. The set of discrete velocities $[\boldsymbol{e}_\alpha]$ was defined as:

$$[\boldsymbol{e}_\alpha] = [\boldsymbol{e}_0, \boldsymbol{e}_1, \ldots, \boldsymbol{e}_8] = \begin{bmatrix} 0 & 1 & 0 & -1 & 0 & 1 & -1 & -1 & 1 \\ 0 & 0 & 1 & 0 & -1 & 1 & 1 & -1 & -1 \end{bmatrix}, \tag{10}$$

and the weight coefficients ω_α can be given by $\omega_0 = 4/9$, $\omega_\alpha = 1/9$ for $\alpha = 1\sim4$ and $\omega_\alpha = 1/36$ for $\alpha = 5\sim8$.

Split-forcing LBE was utilized for higher accuracy which demands the following [32]:

$$F_\alpha(\boldsymbol{x},t) = (1 - \frac{1}{2\tau})\omega_\alpha[3\frac{\boldsymbol{e}_\alpha - \boldsymbol{u}(\boldsymbol{x},t)}{c^2} + 9\frac{\boldsymbol{e}_\alpha\cdot\boldsymbol{u}(\boldsymbol{x},t)}{c^4}\boldsymbol{e}_\alpha]\cdot\boldsymbol{f}(\boldsymbol{x},t). \tag{11}$$

The macroscopic density and velocity at the Euler points can be directly obtained by:

$$\rho = \sum_\alpha f_\alpha, \tag{12}$$

$$\rho\boldsymbol{u} = \sum_\alpha \boldsymbol{e}_\alpha f_\alpha + \frac{\Delta t}{2}\boldsymbol{f}. \tag{13}$$

Fixed Euler grids and deformable Lagrangian grids are both employed in the IB-LB method. Euler grids are fixed grids related to the computation of flow, while Lagrangian grids are distributed on the surface of the particle and move with it, as shown in Figure 1b. The fluid and the immersed boundary can exchange information through these two grids. The force exerted on the Lagrangian points at the surface of the boundary is given by [33]:

$$\boldsymbol{F}(\boldsymbol{x},t) = \frac{\boldsymbol{U}^d(\boldsymbol{x},t+\Delta t) - \boldsymbol{U}^*(\boldsymbol{x},t+\Delta t)}{\Delta t}, \tag{14}$$

where $\boldsymbol{U}^d(\boldsymbol{x}, t)$ is the velocity of the points on the boundary governed by the law of rigid-body motion and $\boldsymbol{U}^*(\boldsymbol{x}, t)$ is the approximate velocity at the position $\boldsymbol{x}$ by interpolating the velocity of the Euler points around the Lagrangian nodes:

$$\boldsymbol{U}^*(\boldsymbol{X}_b,t) = \sum_f D(\boldsymbol{X}_b - \boldsymbol{X}_f)\cdot\boldsymbol{u}^*(\boldsymbol{X}_f,t), \tag{15}$$

where $\boldsymbol{u}^*(\boldsymbol{X}_f, t)$ is the fluid velocity at $\boldsymbol{X}_f$ without considering a forcing term and $\boldsymbol{D}(\boldsymbol{x})$ is the discrete delta function [31].

The forces exerted on the fluid by the moving boundary can be obtained as:

$$f(\boldsymbol{X}_f, t) = \sum_b D(\boldsymbol{X}_f - \boldsymbol{X}_b) \cdot \boldsymbol{F}(\boldsymbol{X}_b, t). \quad (16)$$

In terms of the fluid–wall interaction, the fluid had no slip and no penetration into the wall, and the non-equilibrium extrapolation method was used to calculate the fluid–wall interaction.

2.4. Validation

To validate the independence of the grid size in the simulations, several cases of rod-shaped squirmers swimming towards the wall were conducted at $Re_s = 0.5$. The swimming Reynolds number ($Re_s = B_1 d\rho/2\mu$) represents the ratio of the inertial to viscous forces within the fluid, where ρ, d, B_1 and μ are the fluid density, characteristic length, the constant related to swimming strength and fluid viscosity, respectively. The rod-shaped squirmers were assembled, with two identical squirmers being in contact. The initial orientation of the squirmers was $\theta = -45^\circ$ and the squirmers were released one diameter ($20\Delta x$) away from the wall, as shown in Figure 1. The height of the flow changed from $H = 300\Delta x$ to $H = 800\Delta x$, and the length of the flow was fixed at $L = 800\Delta x$. As shown in Figure 2, the curves of the squirmers' trajectory and orientation variation coincided well when $H > 500\Delta x$. Thus $H = 540\Delta x$ was selected in the simulations for saving computational resources while ensuring the reliability of the simulation results.

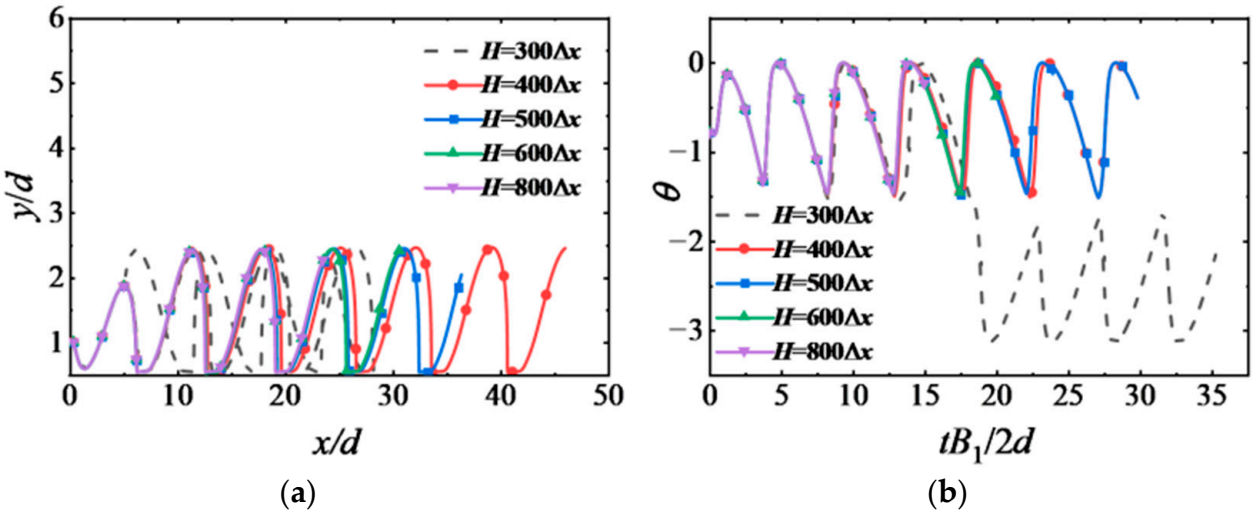

Figure 2. Trajectory and variation in the orientation with time for a rod-shaped squirmer with $\beta = 3$ at $Re_s = 0.5$ (initial angle $\theta = -\pi/4$, $h = d$): (**a**) trajectory and (**b**) orientation.

3. Results and Discussion

The swimming state of different types of rod-shaped squirmer is discussed in terms of the action of the wall at different values of Re_s. As shown in Figure 1, a single rod-shaped squirmer could be made of i two-dimensional cylindrical squirmers connected in series, where s was the distance between adjacent squirmer centroids. The diameter of a single squirmer was $d = 20\Delta x$, and the Lagrange grids of the surface was 150. At the initial moment, the squirmer was placed in the static flow with an azimuth angle of θ, as shown in Figure 1, where the dashed line represents the far-field boundary and the solid line represents the solid wall boundary without sliding and penetration. Moving grid technology was used to ensure that the horizontal position of the mass center of the squirmer rod was located at the center of the flow. When the mass center of the squirmer moved beyond a grid from the horizontal center of the flow, the squirmer and the information of the flow moved horizontally by a grid in the opposite direction. It has been proven that when $L = 40d$ and $H = 27d$, the squirmer's trajectory does not change. Ouyang et al. [19] studied the

effect of the wall surface on squirmer motion with a single squirmer, and found that when the initial distance of the squirmer from the wall changed, the initial collision between the squirmer and the wall was different, but the swimming mode was not changed. In the present study, we found that Ouyang et al.'s conclusion was also applicable to rod-shaped squirmers. Therefore, the influence of the initial azimuth angle and the initial distance from the wall to the rod-shaped squirmer on its swimming state was no longer considered in the present study, and attention was paid to the influence of different centroid spacings of the squirmer s, squirmer numbers i and swimming Reynolds numbers Re_s on the hydrodynamic properties of rod-shaped squirmers. Thus, the initial state of the front squirmer was $\theta = -\pi/4$ and $h = d$ in all simulations. Given the position and azimuth of the front squirmer, the position and attitude of the rod-shaped squirmer could be determined.

3.1. Basic Swimming State and Flow Structure of Rod-Shaped Squirmers

Figure 3 shows the change in the trajectory and azimuth of rod-shaped squirmers with different values of β. It can be seen that four swimming modes appear after the first collision between the squirmer and the wall. (a) The squirmer with $-9 \leq \beta \leq -3$ swims in reverse in the region near the wall, with a negative azimuth angle, accompanied by periodic oscillations of small amplitude. (b) The squirmer with $\beta = -1$ moves forward close to the wall at an azimuth angle close to 0. (c) The squirmer with $0 \leq \beta \leq 1$ swims vertically from the wall at a positive azimuth angle. (d) The squirmer with $3 \leq \beta \leq 7$ swims in the positive direction and makes periodic motions of large amplitude at a certain distance from the wall. Among the above four modes, the latter three swimming modes were observed through experiments and simulations, while the first mode of reverse swimming was less common.

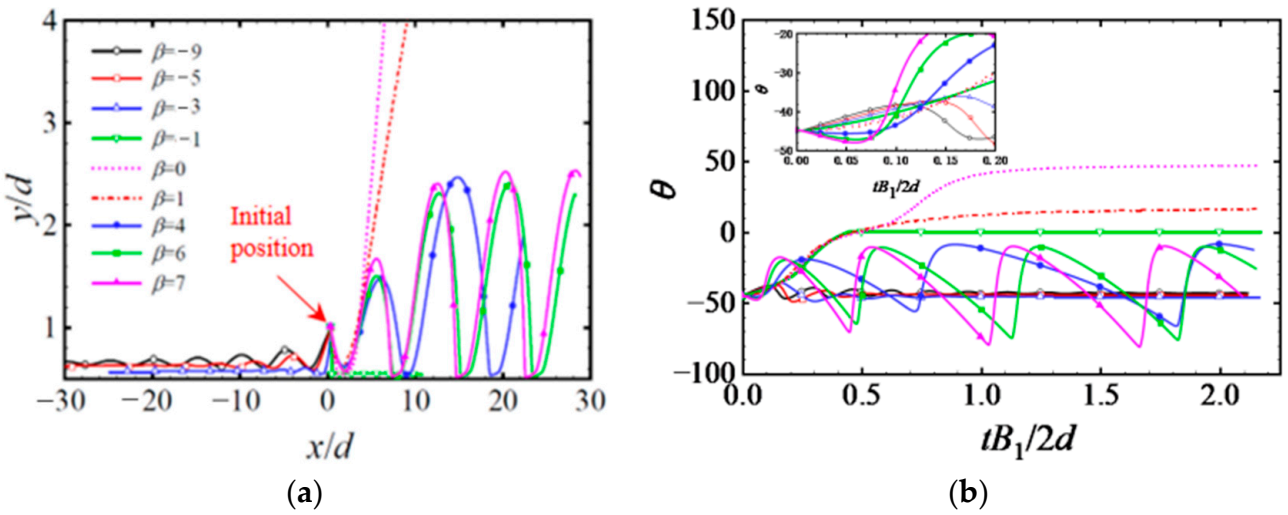

Figure 3. Variations in the (**a**) trajectory and (**b**) azimuth of rod-shaped squirmers with time at different values of β ($Re_s = 0.1$, $s = d$, $i = 2$).

The pusher with a larger β would move in the opposite direction along the surface of a cylinder, with its axis perpendicular to the flow because the vortex generated between the squirmer and the wall exerted a strong force in the opposite direction on the squirmer [20]. This reverse swimming phenomenon can be explained by the far-field approximation theory and the multipole expansion method, i.e., the occurrence of reverse swimming is to satisfy the non-slip boundary condition at the fixed wall. The pressure distribution near the swimmer is helpful for understanding the mechanism of reverse swimming for rod-shaped squirmers, as shown in Figure 4, where the ahead of the pusher ($\beta = -5$) is the region with high pressure, and the rear is the region with low pressure (the unit of pressure is lattice units in the LBM). This pressure distribution will weaken the forward swimming caused by the driving force of the rod-shaped squirmer itself. When the driving force of the rod-shaped squirmer cannot overcome the reverse pressure gradient in the head of the

pusher, the reverse swimming phenomenon may occur. However, the pressure distribution around the puller (β = 5) is opposite to that of the pusher. The head of the puller is the region with low pressure, and the rear is the region with high pressure. Therefore, the rod-shaped squirmer with $\beta > 0$ can maintain a forward swimming state.

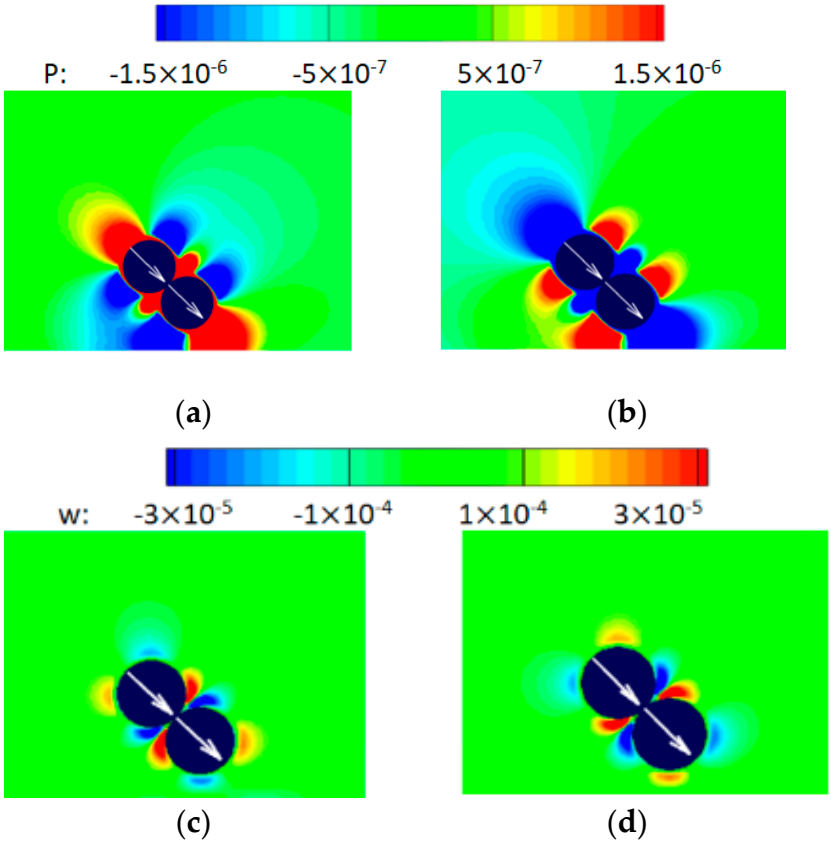

Figure 4. Pressure and vorticity distribution around a rod-shaped squirmer (Re_s = 0.1): (**a**) pressure, $\beta = -5$; (**b**) pressure, $\beta = 5$; (**c**) vorticity, $\beta = -5$; (**d**) vorticity, $\beta = 5$.

Changes in the translational and angular velocity of rod-shaped squirmers with different values of β with time are compared in Figure 5. For the squirmer with $-9 \leq \beta \leq 1$, the swimming velocity stabilized to a fixed value, which increased with an increase in the absolute value of β and was greater than the steady swimming velocity in the infinite flow. For the squirmer with $4 \leq \beta \leq 7$, the swimming velocity always fluctuated within a certain range, which is consistent with the numerical results given by Li and Ardekani [16]. As shown in Figures 3b and 5b, within the period of time before the squirmer collided with the wall for the first time (i.e., the stage of $tB_1/2d$ changing from 0 to 0.20 in the small diagram of Figure 3b), the azimuth angle of the squirmer with $-1 \leq \beta \leq 1$ increased linearly, and the azimuth angle of the pusher ($\beta \leq -3$) or puller ($\beta \geq 4$) increased or decreased first when swimming towards the wall; the rotational angular velocity of the puller was also greater than that of the pusher. The direction of the angular velocity of the squirmer was reversed when the squirmer was about to contact the wall, the azimuth angle of the pusher or puller began to suddenly decrease or increase, and its rate of change increased with the increase in the absolute value of β. Brown et al. [34] and Ouyang et al. [19] indicated that the hydrodynamic effect and degree of collision between squirmer and the wall were different with different values of β, so the magnitude of the change in the squirmer's azimuth before and after collision was different. The degree of attitude transition of the squirmers with different values of β at the wall determines its swimming mode.

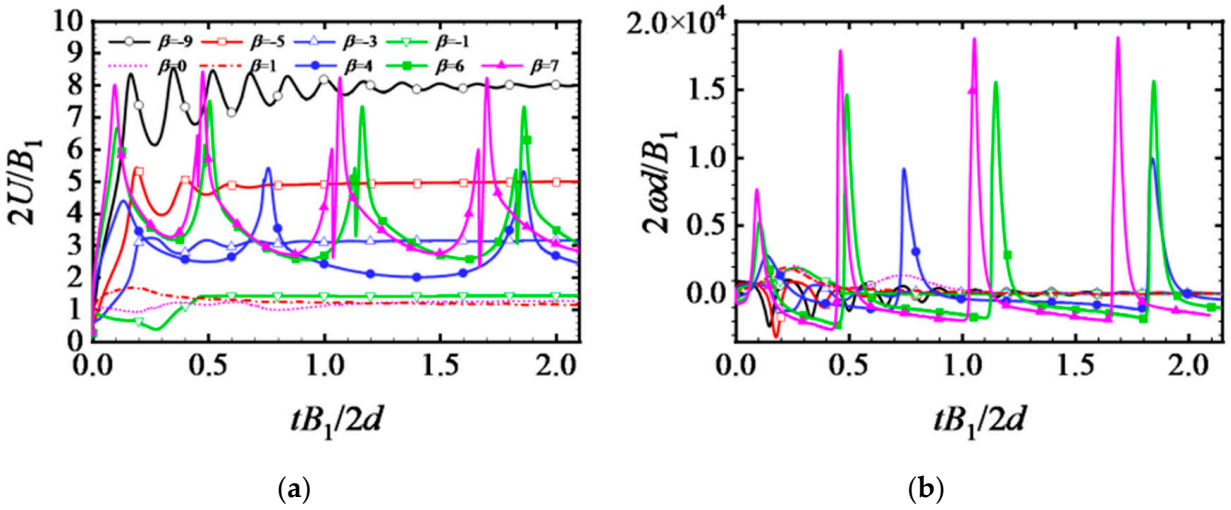

(**a**) (**b**)

Figure 5. Variation in the velocity (**a**) and angular velocity (**b**) of rod-shaped squirmers with time for different values of β (Re_s = 0.1, $s = d$, i = 2).

As shown in Figure 3a, both pushers and pullers displayed the swimming mode of periodic motion, and the amplitude of the periodic motion of the latter was much larger than that of the former. This is because when the puller completed a collision with the wall and started to swim away from the wall, the azimuth angle of the puller increased under the hydrodynamic action, and the trend of swimming toward the wall caused by its own driving force decreased correspondingly.

Figure 6 shows the distribution of flow velocity and the streamline when the pusher, neutral squirmer and puller swam. When a single pusher or puller moved in an infinite flow, there were four clusters of closed streamlines around it. The streamline distribution of pushers and pullers near the wall was similar to that of a single squirmer, but a cluster of closed streamlines near the wall was suppressed (for the pusher with $\beta = -5$) or even disappeared (for the puller with $\beta = 5$), and a small closed streamline in the opposite direction developed between two adjacent squirmer gaps. This was because the pusher formed a positive flow at the gap between the pusher and the wall, while the puller formed a reverse flow at the gap between the puller and the wall, enhancing the development of small vortices at the gap. The streamline distribution obtained in the present study is similar to that given by Yazdi et al. [35] using perturbation theory when a single squirmer moved near the wall. For the neutral squirmer, the streamline around the squirmer was counterclockwise in the large area because the azimuth angle of the neutral squirmer rotated to a proper position and escaped from the wall when it collided with the wall.

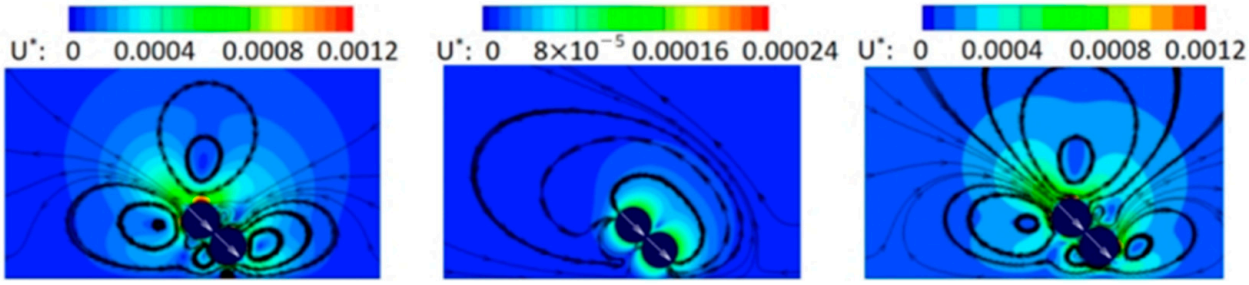

(**a**) (**b**) (**c**)

Figure 6. Distribution of the flow velocity and streamline: (**a**) $\beta = -5$, (**b**) $\beta = 0$, (**c**) $\beta = 5$ (Re_s = 0.1).

3.2. Effect of Re_s

A simulation was conducted with a range of swimming Reynolds numbers, $0.1 \leq Re_s \leq 2.0$, because there are many organisms living in this range. Four other swimming modes of rod-shaped squirmers were found: (a) an octagonal motion, (b) a circular motion, (c) reverse motion away from the wall and (d) motion away from the wall, accompanied by alternating changes from clockwise to anticlockwise. The trajectories of rod-shaped squirmers at different values of Re_s are compared in Figure 7. For a pusher ($\beta = -5$), its swimming mode changed from reverse swimming with periodic oscillation to reverse moving away from the wall when Re_s changed from 0.1 to 1.0. The amplitude of the periodic motion of the pusher increased gradually when Re_s increased, and the periodic motion transformed into a reverse motion away from the wall when the amplitude of the pusher increased to a certain extent and it collided with the wall in a particular position at a certain time. The neutral squirmer retained its vertical motion away from the wall when Re_s increased, but the slope of the trajectory increased with an increase in the Re_s. In Newtonian fluid, Re_s only affects the trajectory of squirmers without changing the motion mode [19]. Figure 7b shows the trajectory of the pullers with $\beta = 1$ and $\beta = 5$. For the puller with $\beta = 1$, its trajectory transformed from a motion away from the wall to a periodic motion, and the period and amplitude of the periodic motion decreased with an increase in the Re_s, which is similar to the results given by Li and Ardekani [16]. The change in the trajectory of the puller with Re_s was opposite to that of the pusher, and inertia weakened the attraction to the pusher and enhanced the attraction to the pusher with a small β. When Re_s increased, the puller with $\beta = 5$ displayed periodic motion, an octagonal motion and circular motion in turn. Dustan et al. [11] studied the motion of microorganisms on the wall using a model of two balls connected by a rod, and found a similar mode, where squirmers moved in a circle at a certain distance from the wall.

Figure 7c shows two types of circular motion, i.e., when the trajectory and rotation direction of the rod-shaped squirmer are clockwise circular motions ($\beta = 7$, $Re_s = 0.5$ and $\beta = 7$, $Re_s = 1.0$), and when the trajectory and rotation direction of the rod-shaped squirmer are both anticlockwise circular motions ($\beta = 6$, $Re_s = 2.0$). The puller ($\beta = 7$, $Re_s = 1.0$) always kept moving in a circle in one area, which would be conducive to the formation of biofilms in nature. The puller ($\beta = 6$, $Re_s = 2.0$) moved in a direction parallel to the wall while making a circular motion. The influence of inertia led to this difference. For the puller, there was a transition region between the two modes of periodic motion near the wall and circular motion, as shown in the area surrounded by the red dotted line in Figure 8. Octagonal motion, and the motion away from the wall accompanied by alternating clockwise and anticlockwise transformation are two transition states, as shown in Figure 7d.

For systematically analyzing the influence of Re_s on the motion mode of squirmer, the motion mode of the squirmer for $0.1 \leq Re_s \leq 2.0$ and $-9 \leq \beta \leq 9$ is summarized in Figure 8. It can be seen that Re_s has an obvious effect on the motion mode of the squirmer. The puller with a large β often showed the circular motion mode. As Re_s increased, the puller with a relatively small β also showed the circular motion mode. For the pusher, no circular motion mode was found. In order to reveal the possible reasons for this mode, without losing generality, the influencing mechanism of inertia on the motion mode of the pusher and puller ($i = 2$, $s = d$) was analyzed. At a finite Re_s, the flow state at the previous time affects the motion of the squirmer at the current time, as shown by the blue solid arrow in Figure 9, where the red arrow indicates the influence of the direction of the flow on the deflected squirmer. It can be seen that when the angle of the puller was shifted by a small disturbance during its movement, the flow at the previous moment pulled the puller away from the original position, causing a greater rotational tendency and eventually making the puller revolve on its own axis. This rotation on its own axis was the cause of its circular motion. When β increased, the vorticity intensity also increased, which enhanced the influence of inertia on the puller's motion. Therefore, when Re_s or β increased, the puller tended to move in a circle. However, for a pusher, the flow at the previous time pushed the deflected pusher back to the original position, so that the pusher did not have

a great rotation tendency. Even if Re_s increased, the circular motion mode of pusher did not appear.

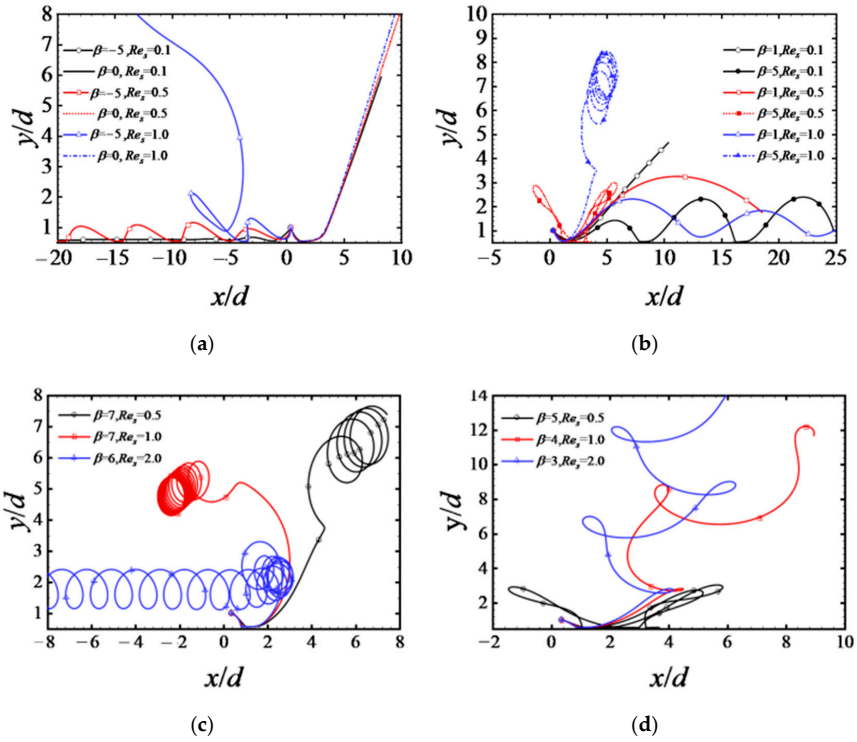

Figure 7. Trajectory of rod-shaped squirmers at different values of Re_s ($s = d$, $i = 2$): (**a**) $\beta = -5$, $\beta = 0$; (**b**) $\beta = 1$, $\beta = 5$; (**c**) a circular motion; (**d**) motion trajectories of two transition states, i.e., octagonal motion, and the motion away from the wall accompanied by alternating clockwise and anticlockwise transformation.

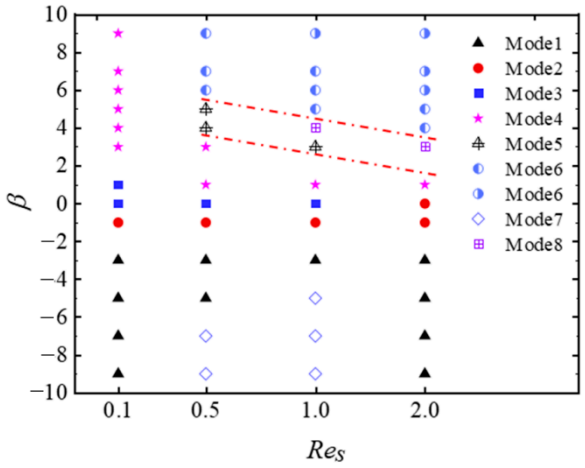

Figure 8. Motion mode of rod-shaped squirmers at different values of Re_s and β ($s = d$, $i = 2$). Mode 1: reverse swimming near the wall with periodic oscillation; Mode 2: close to the wall and moving forward; Mode 3: swimming forward away from the wall; Mode 4: positive swimming near the wall with periodic oscillation; Mode 5: octagonal motion; Mode 6: circular motion, where the left-hand solid circle indicates that the trajectory and rotation direction of the squirmer are both clockwise, and the right-hand solid circle indicates that the trajectory and rotation direction are both counterclockwise; Mode 7: reverse swimming away from the wall; Mode 8: swimming away from the wall with alternating clockwise and anticlockwise transformation. The red dotted line indicates the area of mode transition.

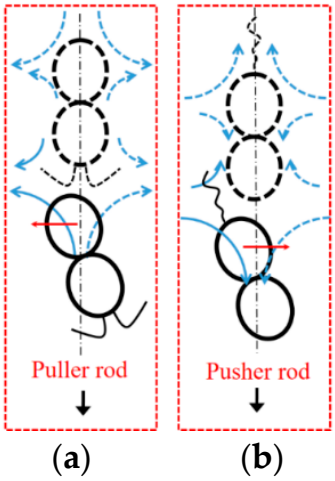

Figure 9. Mechanism of the rotation tendency of a pusher and a puller at a finite Re_s: (**a**) puller; (**b**) pusher ($s = d$, $i = 2$). The black dotted line and the solid line represent the squirmer at the previous time and the current time, respectively. The blue arrow indicates the flow generated by the squirmer at the previous time, and the solid arrow indicates the influence of the flow at the previous time on the squirmer's motion at the current time. The red arrow indicates the influence of the direction of the flow on the deflected squirmer.

The change in the motion mode of a squirmer can also be reflected in phase space, as shown in Figure 10. For the pusher with $\beta = -3$, its trajectory in phase space eventually became stable as a circle of finite size, and the area of the circular region increased with an increase in Re_s, so increasing the Re_s led to dynamic instability. For the puller with $\beta = 3$ and the neutral squirmer with $\beta = 0$, the trajectories in phase space changed morphologically with an increase in Re_s, corresponding to the change in the motion mode of the squirmer. For the squirmer with $\beta = 7$ in a circular motion, the trajectories in phase space were disordered and difficult to describe. Lauga et al. [7] indicated that the circular trajectory of microorganisms is a natural swimming mode without force and torque under the hydrodynamic action of the wall. Here, we found that although the circular motion of the squirmer was relatively stable, it also rotated continuously.

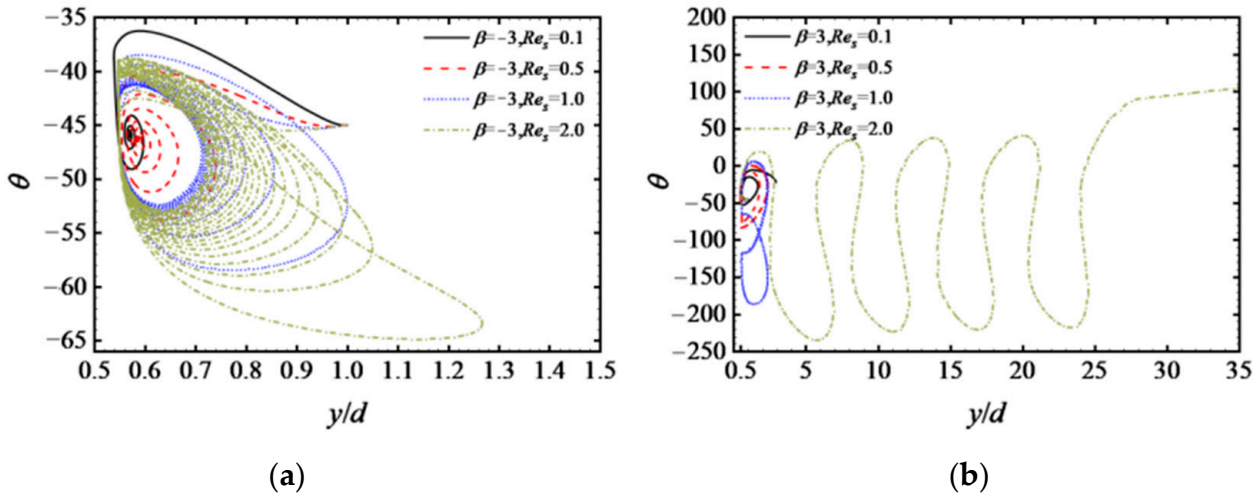

Figure 10. *Cont.*

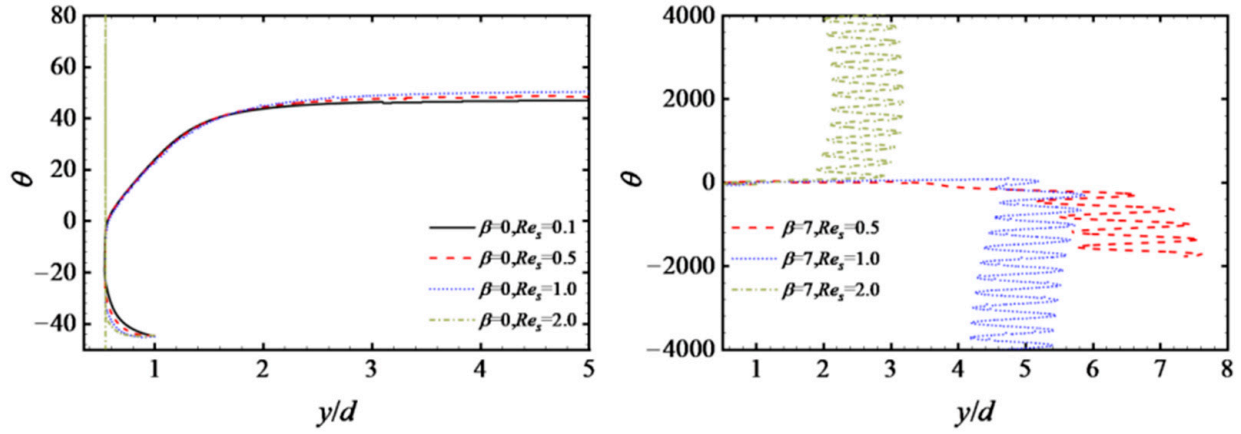

Figure 10. Phase diagram of the trajectory of rod-shaped squirmers at different values of Re_s ($s = d$, $i = 2$): (**a**) $\beta = -3$; (**b**) $\beta = 3$; (**c**) $\beta = 0$; (**d**) $\beta = 7$.

3.3. Effect of the Number of Assembled Squirmers i

The trajectories of rod-shaped squirmers with $i = 2, 3, 4$ are shown in Figures 11 and 12. As shown in Figures 11a and 12a, the neutral squirmer moved away from the wall. With an increase in i, the first collision time of the neutral squirmer became longer and the stable azimuth of the squirmer decreased after the collision. The pusher with $\beta = -1$ moved forward and was close to the wall for $i = 2, 3$, but kept away from the wall after the collision with the wall and the azimuth angle kept increasing for $i = 4$. As shown in Figures 11b and 12b, the puller with $\beta = 3$ moved periodically along the wall, and the amplitude of the periodic motion slightly decreased and the period increased with an increase in i. The puller with $\beta = 6$ made an octagonal motion for $i = 3, 4$, but made a circular motion for $i = 2$.

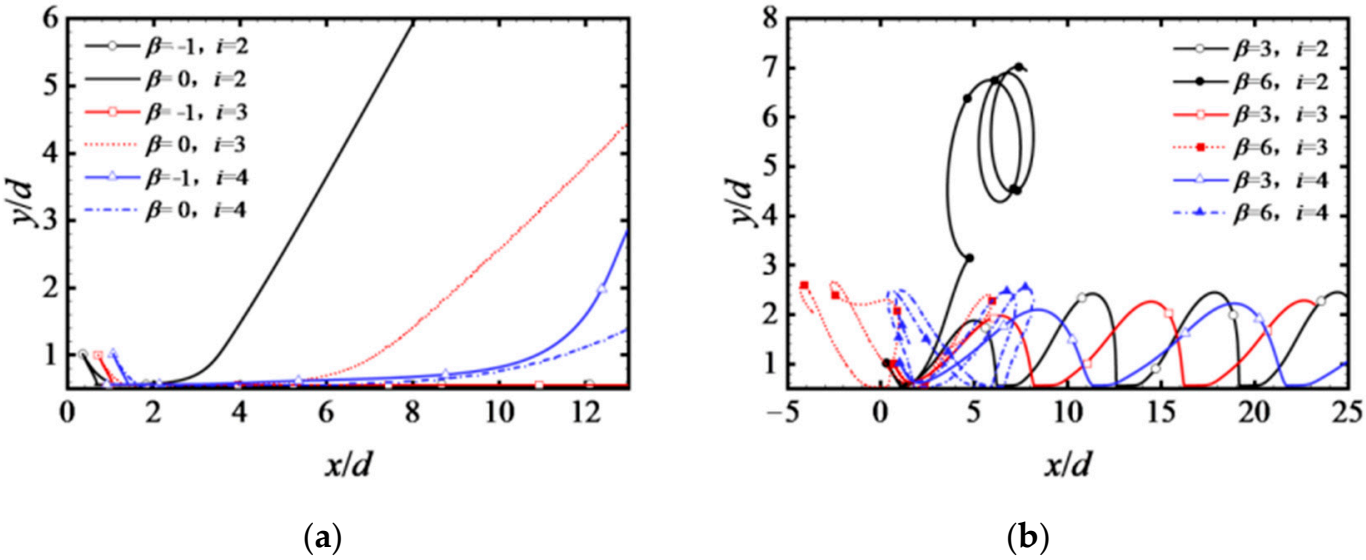

Figure 11. Trajectory of rod-shaped squirmers with different values of i ($Re_s = 0.5$, $s = d$): (**a**) $\beta = -1$ and $\beta = 0$; (**b**) $\beta = 3$ and $\beta = 6$.

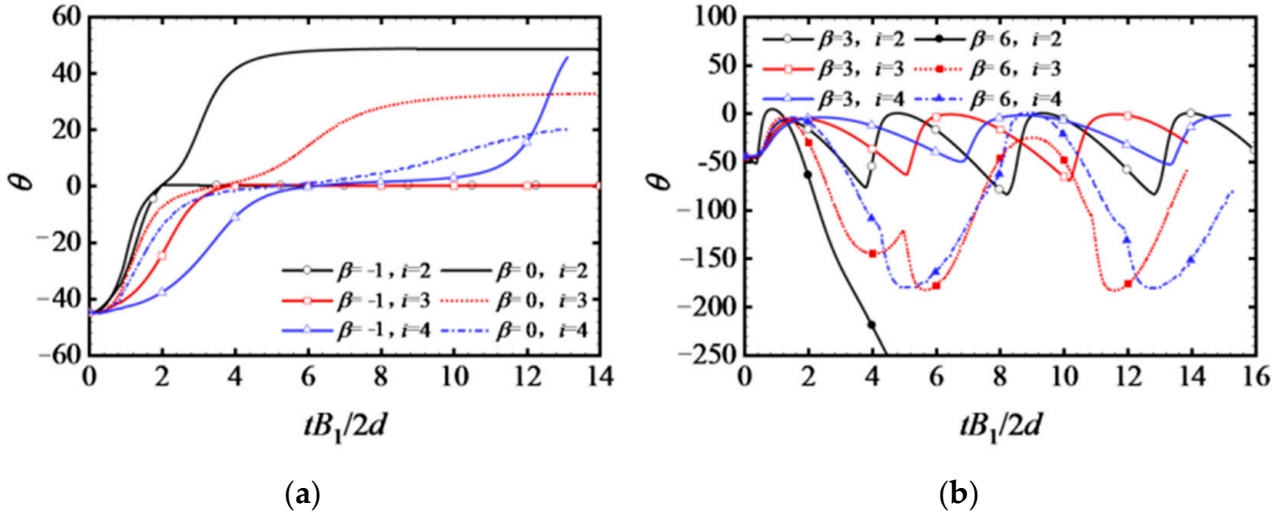

Figure 12. Change in the azimuth of rod-shaped squirmers with different values of i (Re_s = 0.5, $s = d$): (**a**) $\beta = -1$ and $\beta = 0$; (**b**) $\beta = 3$ and $\beta = 6$.

Ouyang and Phan-Thien [36] studied the motion of rod-shaped squirmers in an infinite flow, and found that the larger i is, the less likely the squirmer is to deviate from the original swimming direction. However, the present results showed that the rod-shaped squirmer rotated under the action of the wall, and the degree of the effect of the flow at the previous moment on the squirmer's motion was different for squirmer with different values of i. The difference in the flow structure around the squirmer and its own inertia (mass, moment of inertia) resulted in a greater rotational tendency of the squirmer with small values of i and was more likely to display the form of circular motion.

3.4. Effect of Adjacent Squirmer Spacing s

The trajectories of rod-shaped squirmers with adjacent squirmer spacing $s = 0.75d$, d and $1.5d$ are shown in Figure 13, where the change in s only affects the trajectory of the squirmer without changing its motion mode. The neutral squirmer showed a motion mode away from the wall, and the collision time of the squirmer with the wall increased with an increase in s. The puller with $\beta = 7$ made a circular motion, and the larger s was, the larger the radius of the circumferential trajectory was.

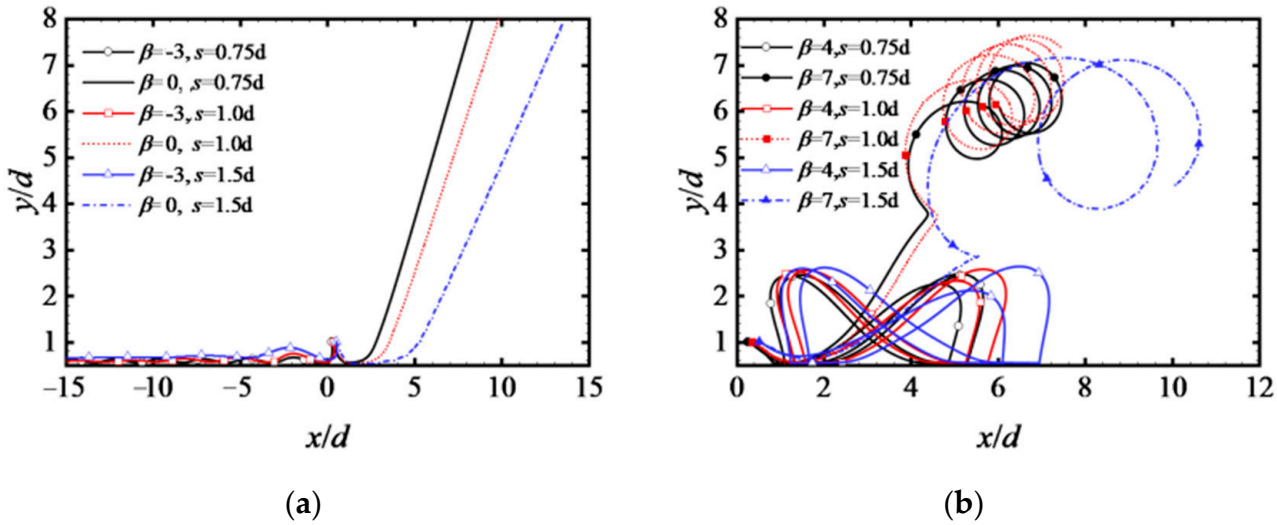

Figure 13. Trajectory of rod-shaped squirmers with different values of s (Re_s = 0.5, i = 2): (**a**) $\beta = -3$ and $\beta = 0$; (**b**) $\beta = 4$ and $\beta = 7$.

The changes in the velocity of rod-shaped squirmers with different values of s are shown in Figure 14. For the pusher with $\beta = -3$, the larger s was, the smaller the swimming velocity was, but the change trend of velocity with s was opposite for the puller with $\beta = 9$. This is attributed to the fact that the vorticity between adjacent squirmers was suppressed when s changed, which affected the effect of inertia. The movement mode of squirmers changed when Re_s or i changed, but the mode did not change when s changed. The reason is that, as shown in Figure 15, the moment of the squirmer caused by the flow at the previous moment is larger when s increases, but its own moment of inertia is also larger, which results in similar rotational tendencies and ensures the stability of the swimming mode when s changes.

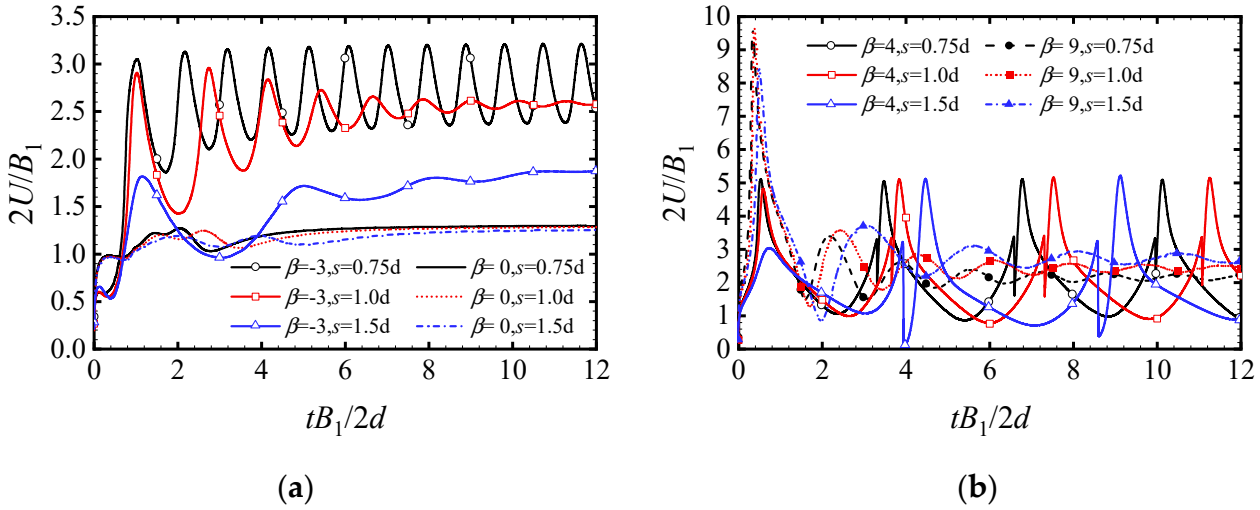

Figure 14. Change in the velocity of rod-shaped squirmers with different values of s ($Re_s = 0.5$, $i = 2$): (**a**) $\beta = -3$ and $\beta = 0$; (**b**) $\beta = 4$ and $\beta = 7$.

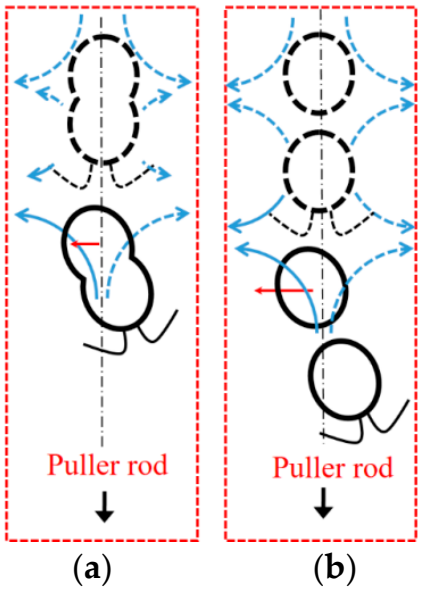

Figure 15. Mechanism of the rotational tendency of pushers and pullers with different values of s: (**a**) $s = 0.75d$; (**b**) $s = 1.5d$.

4. Conclusions

The hydrodynamic characteristics and swimming mode of a rod-shaped squirmer swimming near a wall at a finite Reynolds number were studied numerically using the immersed boundary-lattice Boltzmann method. The swimming behavior of squirmer

and the flow structure are presented, and the effect of the distance between two adjacent squirmers, the number of assembled squirmers and the Reynolds number on the swimming mode of the squirmers was explored. The main conclusions are summarized as follows:

(1) There are four swimming modes after the first collision between the squirmer and the wall, i.e., (a) swimming reversely in the region near the wall with a negative azimuth angle, accompanied by periodic oscillations of small amplitude; (b) moving forward close to the wall at an azimuth angle close to 0; (c) swimming vertically from the wall at a positive azimuth angle; (d) swimming in the positive direction and making periodic motions with a large amplitude at a certain distance from the wall.

(2) There are four swimming modes when Re_s changes from 0.1 to 2.0, i.e., (a) an octagonal motion, (b) a circular motion, (c) reverse motion away from the wall and (d) motion away from the wall accompanied by alternating clockwise and anticlockwise transformation.

(3) Puller, pusher and neutral squirmers show different swimming modes when the number of assembled squirmers i changes. Rod-shaped squirmers will rotate through the action of the wall, and the degree of the effect of the flow at the previous moment on the squirmer's motion is different for different values of i. The difference in the flow structure around the squirmer and its own inertia results in greater rotational tendency of the squirmer with a small i and is more likely to appear in the form of circular motion.

(4) The change in the distance between two adjacent squirmers s only affects the trajectory of the squirmer without changing its motion mode. Puller, pusher and neutral squirmers show different swimming modes and velocity changes when s changes.

Author Contributions: Conceptualization, H.Y.; methodology, Z.O.; software, H.Y. and Z.O.; validation, H.Y.; formal analysis, H.Y.; investigation, H.Y., and J.L.; resources, H.Y. and Z.O. and J.L.; data curation, H.Y.; writing—original draft preparation, H.Y.; writing—review and editing, J.L.; visualization, H.Y.; supervision, J.L.; project administration, J.L.; funding acquisition, J.L. All authors have read and agreed to the published version of the manuscript.

Funding: National Natural Science Foundation of China (Grant 12132015).

Institutional Review Board Statement: Not applicable.

Informed Consent Statement: Not applicable.

Data Availability Statement: Data sharing not applicable.

Conflicts of Interest: The authors declare no conflict of interest.

References

1. Lauga, E.; Powers, T.R. The hydrodynamics of swimming microorganisms. *Rep. Prog. Phys.* **2009**, *72*, 096601. [CrossRef]
2. Suarez, S.S.; Pacey, A.A. Sperm transport in the female reproductive tract. *Hum. Reprod. Update* **2006**, *12*, 23–37. [CrossRef] [PubMed]
3. Berg, H.C.; Anderson, R.A. Bacteria swim by rotating their flagellar filaments. *Nature* **1973**, *245*, 380–382. [CrossRef]
4. Shields, R. Cell Movements. *Nature* **1975**, *5504*, 107. [CrossRef]
5. Drescher, K.; Leptos, K.C.; Tuval, I.; Ishikawa, T.; Pedley, T.J.; Goldstein, R.E. Dancing volvox: Hydrodynamic bound states of swimming algae. *Phys. Rev. Lett.* **2009**, *102*, 168101. [CrossRef]
6. Miki, K.; Clapham, D.E. Rheotaxis guides mammalian sperm. *Curr. Biol.* **2013**, *23*, 443–452. [CrossRef]
7. Lauga, E.; DiLuzio, W.R.; Whitesides, G.M.; Stone, H.A. Swimming in circles: Motion of bacteria near solid boundaries. *Biophys. J.* **2006**, *90*, 400–412. [CrossRef]
8. Harshey, R.M. Bacterial motility on a surface: Many ways to a common goal. *Annu. Rev. Microbiol.* **2003**, *57*, 249–273. [CrossRef]
9. Or, Y.; Murray, R.M. Dynamics and stability of a class of low Reynolds number swimmers near a wall. *Phys. Rev. E Stat. Nonlinear Soft Matter Phys.* **2009**, *79*, 045302. [CrossRef]
10. Zargar, R.; Najafi, A.; Miri, M. Three-sphere low-Reynolds-number swimmer near a wall. *Phys. Rev. E Stat. Nonlinear Soft Matter Phys.* **2009**, *80*, 026308. [CrossRef]
11. Dunstan, J.; Miño, G.; Clement, E.; Soto, R. A two-sphere model for bacteria swimming near solid surfaces. *Phys. Fluids* **2012**, *24*, 011901. [CrossRef]
12. Pimponi, D.; Chinappi, M.; Gualtieri, P.; Casciola, C.M. Hydrodynamics of flagellated microswimmers near free-slip interfaces. *J. Fluid Mech.* **2016**, *789*, 514–533. [CrossRef]

13. Di Leonardo, R.; Dell'Arciprete, D.; Angelani, L.; Iebba, V. Swimming with an image. *Phys. Rev. Lett.* **2011**, *106*, 038101. [CrossRef] [PubMed]
14. Papavassiliou, D.; Alexander, G.P. The many-body reciprocal theorem and swimmer hydrodynamics. *Europhys. Lett.* **2015**, *110*, 44001. [CrossRef]
15. Lintuvuori, J.S.; Brown, A.T.; Stratford, K.; Marenduzzo, D. Hydrodynamic oscillations and variable swimming speed in squirmers close to repulsive walls. *Soft Matter* **2016**, *12*, 7959–7968. [CrossRef]
16. Li, G.J.; Ardekani, A.M. Hydrodynamic interaction of microswimmers near a wall. *Phys. Rev. E Stat. Nonlinear Soft Matter Phys.* **2014**, *90*, 013010. [CrossRef]
17. Ishimoto, K.; Gaffney, E.A. Squirmer dynamics near a boundary. *Phys. Rev. E* **2013**, *88*, 062702. [CrossRef]
18. Poddar, A.; Bandopadhyay, A.; Chakraborty, S. Near-wall hydrodynamic slip triggers swimming state transition of micro-organisms. *J. Fluid Mech.* **2020**, *894*, A11. [CrossRef]
19. Ouyang, Z.Y.; Lin, J.Z.; Ku, X.K. Hydrodynamic properties of squirmer swimming in power-law fluid near a wall. *Rheol. Acta* **2018**, *57*, 655–671. [CrossRef]
20. Kuron, M.; Stark, P.; Holm, C.; de Graaf, J. Hydrodynamic mobility reversal of squirmers near flat and curved surfaces. *Soft Matter* **2019**, *15*, 5908–5920. [CrossRef]
21. Pietrzyk, K.; Nganguia, H.; Datt, C.; Zhu, L.L.; Elfring, G.J.; Pak, O.S. Flow around a squirmer in a shear-thinning fluid. *J. Non-Newton. Fluid Mech.* **2019**, *268*, 101–110. [CrossRef]
22. Eastham, P.S.; Shoele, K. Axisymmetric squirmers in Stokes fluid with nonuniform viscosity. *Phys. Rev. Fluids* **2020**, *5*, 063102. [CrossRef]
23. van Gogh, B.; Demir, E.; Palaniappan, D.; Pak, O.S. The effect of particle geometry on squirming through a shear-thinning fluid. *J. Fluid Mech.* **2022**, *983*, A3. [CrossRef]
24. Ouyang, Z.Y.; Lin, J.Z. The hydrodynamics of an inertial squirmer rod. *Phys. Fluids* **2021**, *33*, 073302. [CrossRef]
25. Ouyang, Z.Y.; Lin, Z.W.; Yu, Z.S.; Lin, J.Z.; Phan-Thien, N. Hydrodynamics of an inertial squirmer and squirmer dumbbell in a tube. *J. Fluid Mech.* **2022**, *939*, A32. [CrossRef]
26. Ouyang, Z.Y.; Lin, J.Z.; Ku, X.K. Hydrodynamic interaction between a pair of swimmers in power-law fluid. *Int. J. Non-Linear Mech.* **2019**, *108*, 72–80. [CrossRef]
27. Lighthill, M.J. On the squirming motion of nearly spherical deformable bodies through liquids at very small reynolds numbers. *Commun. Pure Appl. Math.* **1952**, *5*, 109–118. [CrossRef]
28. Blake, J.R. A spherical envelope approach to ciliary propulsion. *J. Fluid Mech.* **1970**, *46*, 199–213. [CrossRef]
29. Glowinski, R.T.; Pan, W.; Hesla, T.I.; Joseph, D.D.; Périaux, J. A Fictitious domain approach to the direct numerical simulation of incompressible viscous flow past moving rigid bodies: Application to particulate flow. *J. Comput. Phys.* **2001**, *169*, 363–426. [CrossRef]
30. Dupuis, A.; Chatelain, P.; Koumoutsakos, P. An immersed boundary–lattice-Boltzmann method for the simulation of the flow past an impulsively started cylinder. *J. Comput. Phys.* **2008**, *227*, 4486–4498. [CrossRef]
31. Kang, S.K.; Hassan, Y.A. A comparative study of direct-forcing immersed boundary-lattice Boltzmann methods for stationary complex boundaries. *Int. J. Numer. Methods Fluids* **2011**, *66*, 1132–1158. [CrossRef]
32. Guo, Z.; Zheng, C.; Shi, B. Discrete lattice effects on the forcing term in the lattice Boltzmann method. *Phys. Rev. E Stat. Nonlinear Soft Matter Phys.* **2002**, *65*, 046308. [CrossRef] [PubMed]
33. Ouyang, Z.Y.; Lin, J.Z.; Ku, X.K. The hydrodynamic behavior of a squirmer swimming in power-law fluid. *Phys. Fluids* **2018**, *30*, 083301. [CrossRef]
34. Brown, A.T.; Vladescu, I.D.; Dawson, A.; Vissers, T.; Schwarz-Linek, J.; Lintuvuori, J.S.; Poon, W.C. Swimming in a crystal. *Soft Matter* **2016**, *12*, 131–140. [CrossRef] [PubMed]
35. Yazdi, S.; Ardekani, A.M.; Borhan, A. Locomotion of microorganisms near a no-slip boundary in a viscoelastic fluid. *Phys. Rev. E Stat. Nonlinear Soft Matter Phys.* **2014**, *90*, 043002. [CrossRef]
36. Ouyang, Z.Y.; Phan-Thien, N. Inertial swimming in a channel filled with a power-law fluid. *Phys. Fluids* **2011**, *33*, 113312. [CrossRef]